Frequency-domain modeling of unshielded multiconductor power cables for periodic excitation with new experimental protocol for wide band parameter identification

Tamiris G. Bade, James Roudet, Jean-Michel Guichon, Carlos A. F. Sartori, Patrick Kuo-Peng, Jean-Luc Schanen, Alexis Derbey

https://doi.org/10.1007/s00202-019-00780-2

Frequency-domain modeling of unshielded multiconductor power cables for periodic excitation with new experimental protocol for wide band parameter identification

Tamiris G. Bade[1] · James Roudet[1] · Jean-Michel Guichon[1] · Carlos A. F. Sartori[2,3] · Patrick Kuo-Peng[4] · Jean-Luc Schanen[1] · Alexis Derbey[1]

Abstract
A complete modeling technique for unshielded power cables is proposed. The focus is on applications where the resonance phenomena take place in electrically long cables and is originated from periodic excitation, such as power converters. The resonance problems caused by switching converters tend to become more common with the advent of wide band gap semiconductors. This paper includes a new experimental protocol specific for unshielded power cable parameter identification in a wide frequency band, from DC up to medium frequencies (tens of MHz), with an impedance analyzer. It also introduces a frequency-domain simulation tool with conversion to the time domain, via the Fourier series. This frequency-domain modeling is straightforward, and its accuracy depends only on the accuracy of the cable parameter identification.

Keywords Unshielded cable · Cable parameters · Impedance analyzer · Cable modeling · Frequency domain

1 Introduction

Cable resonance is a well-known phenomenon that may considerably compromise an electrical installation safety. In the literature, we can find numerous applications where cable resonance causes system dysfunctions, e.g., the connection between motors and its drives [17,23,25], the feeding line of high speed trains [4], the connection between an offshore generator station and onshore power converters [28,36] and the switching of protective devices in power systems [2]. These problems tend to become more dangerous with the advent of wide band gap semiconductor technology [11], which have faster switching time.

Long cables can be modeled as transmission lines, in the frequency and time domains. The latter allows the inclusion of nonlinear devices and is useful for real-time applications, which is why it is preferred in the literature and in power system modeling software such as EMTP. However, as the cable parameters are frequency dependent, approximations are often needed to accurately represent the cable behavior. Frequency-domain simulation can represent this dependency accurately, as is the case of the modeling based on the numerical Laplace transform [10], which is convenient for aperiodic excitation.

Particularly, in the cases where resonance takes place in the cable, the representation of the loss-related parameters per-unit-length (p.u.l.) resistance R and P.U.L. conductance G in function of frequency has a great impact on the results [32]. A wide variety of equivalent circuits that emulate the frequency dependence of the losses on time-domain simulation is proposed in the literature, such as T-ladder networks [16,33] or circuits derived from Padé approximations [29]. These can be applied for multiconductor cables [16]; however, the numerically determined equivalent circuits might be unstable [22]. Also, their computation time increases with the cable length.

A frequency-domain modeling requires the identification of the cable parameters in function of the frequency.

✉ Tamiris G. Bade
tamiris.grossl-bade@g2elab.grenoble-inp.fr

1 CNRS, Grenoble INP, G2Elab, Univ. Grenoble Alpes, 38000 Grenoble, France

2 Escola Politécnica da Universidade de São Paulo (PEA/EPUSP), São Paulo, SP 05508-010, Brazil

3 Instituto de Pesquisas Energéticas e Nucleares (IPEN/CNEN-SP), São Paulo, SP 05508-900, Brazil

4 GRUCAD, University of Santa Catarina, Florianópolis, Brazil

There are numerous identification techniques in the literature, using either analytical solutions, numerical methods or line parameters extraction from frequency- and/or time-domain measurements.

Analytical solution derived directly from Maxwell equations [24,30] is possible for unshielded cables in a homogeneous media, and if its geometry can be easily described in some coordinate system. As for numerical methods, many techniques are available [7,8,13,14,21]. Its inconveniences are widely known: high computational effort, the need of an accurate description of the geometry and/or the physical constants linked to the problem. Moreover, for both analytical and numerical methods, measurements are necessary to an accurate determination of physical parameters of the materials. For the low frequency cables used in the applications aforementioned, the measurements needed for a direct parameter identification are not more difficult than measuring the relative permittivity of the cable insulation, for example.

The transmission line parameters can be extracted directly from frequency-domain measurements using impedance analyzers [3,20] or vector network analyzers (VNA) [19, 31,34,35]. VNA-based parameter assessment techniques are extensively used for connections on printed circuit boards and can be extended to power cables [35], for any frequency band within the VNA frequency range. Furthermore, additional time-domain reflectometer (TDR) measurements allow the inclusion of low frequency parameters to the VNA-based cable parameter identification [19]. Impedance analyzer measurements [3,20] are also efficient and well suited for low frequencies.

In this paper, a complete modeling technique is proposed for unshielded long cables susceptible to resonance phenomenon, including the cable parameter identification and modeling. Because many of the systems in which resonance takes place have power converter harmonics exciting the cable, unshielded cables with periodic excitation are the focus of this paper.

The cable parameters are identified with an impedance analyzer, in a wide frequency band: from DC up to tens of MHz. The precautions needed to be taken with unshielded cables at this frequency band are not yet published in the literature. The accuracy of the parameters obtained following proposed protocol is validated with frequency- and time-domain experiments.

The cable is modeled and simulated in the frequency domain, in the steady-state sinusoidal regime. The power converters are represented on the frequency domain using piece-wise linear models [10,26,27], along with the Fourier series associated with the phasor transform. The results can be converted to time domain and are experimentally validated. The proposed frequency-domain model is an improvement of the model proposed in [22].

This paper is structured as follows: Section 2 defines the frequency-domain model, Sect. 3 describes the impedance analyzer measurements needed to identify the cable parameters, Sect. 4 proposes a measurement protocol to guarantee their accuracy, and Sects. 5 and 6 describe the validation experiments on frequency and time domains, respectively.

2 Transmission line frequency-domain model

This section contains brief recall on the multiconductor transmission line theory, as it has been exhaustively studied in the literature. The equations needed to develop a frequency-domain simulator for a multiconductor transmission line (MTL) are written.

The MTL on the schematic in Fig. 1 has $n+1$ conductors, and its geometry is constant along the axis z. It can be modeled on the frequency domain using the chain matrix representation of a transmission line with Eq. (1) [24].

$$\begin{bmatrix}\mathbf{V}(z)\\ \mathbf{I}(z)\end{bmatrix} = \begin{bmatrix}\mathbf{\Phi}_1(z) & \mathbf{\Phi}_2(z)\\ \mathbf{\Phi}_3(z) & \mathbf{\Phi}_4(z)\end{bmatrix}\begin{bmatrix}\mathbf{V}(0)\\ \mathbf{I}(0)\end{bmatrix} \tag{1}$$

$$\mathbf{\Phi}_1(z) = \mathbf{Z}_c \cosh(z\sqrt{\mathbf{YZ}})\mathbf{Y_c} \tag{2}$$

$$\mathbf{\Phi}_2(z) = -\mathbf{Z}_c \sinh(z\sqrt{\mathbf{YZ}}) \tag{3}$$

$$\mathbf{\Phi}_3(z) = -\sinh(z\sqrt{\mathbf{YZ}})\mathbf{Y_c} \tag{4}$$

$$\mathbf{\Phi}_4(z) = \cosh(z\sqrt{\mathbf{YZ}}) \tag{5}$$

In Eqs. (1), (2), $\mathbf{V}$ and $\mathbf{I}$ are vectors of size n containing, respectively, the phasor voltages and currents of each active conductor related to the reference conductor. $\mathbf{Z}_c = \mathbf{Y}^{-1}\sqrt{\mathbf{YZ}}$ is the characteristic impedance matrix,$\mathbf{Y}_c = \mathbf{Z}_c^{-1}$ is the characteristic admittance matrix, and $\sqrt{\mathbf{YZ}}$ is the non-diagonalized propagation matrix. Matrix $\mathbf{Z} = \mathbf{R} + j\omega\mathbf{L}$ is the p.u.l. impedance matrix, and $\mathbf{Y} = \mathbf{G} + j\omega\mathbf{C}$ is the p.u.l. admittance matrix. The definition of matrices $\mathbf{R}$ (p.u.l.resistances), $\mathbf{L}$ (p.u.l. inductance),$\mathbf{G}$ (p.u.l. conductance) and $\mathbf{C}$ (p.u.l.

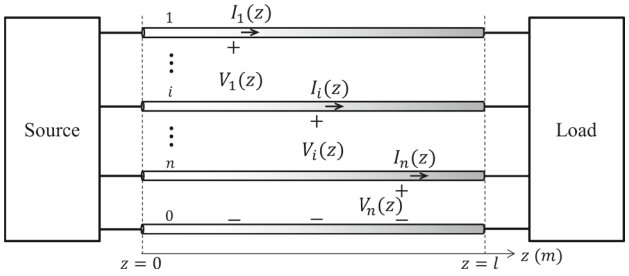

Fig. 1 Generic multiconductor transmission line

capacitance) can be found in [24]; j is the imaginary unity, and ω is the angular frequency.

The voltage/current relation at the line terminals can be expressed with a generalization of the Norton theorem for a $n+1$ port device [15]:

$$\mathbf{I}(0) = \mathbf{I_S} + \mathbf{Y}_S\mathbf{V}(0) \tag{6}$$

$$\mathbf{I}(\ell) = \mathbf{I_L} + \mathbf{Y}_L\mathbf{V}(\ell) \tag{7}$$

where $\mathbf{I_S}$ and $\mathbf{I_L}$ are current source vectors, and $\mathbf{Y}_S$ and $\mathbf{Y}_L$ are the input admittance matrix representing the devices "Source" and "Load," respectively, in Fig. 1.

Equations (1), (6) and (7) are enough to obtain a solution for voltages and currents along the line. The solution of these equations will be henceforth called the "frequency-domain simulator." This is a length-scalable, straightforward cable modeling, because the p.u.l. parameters can be directly injected in the model.

3 Parameter identification using impedance analyzer

Two quasi-equivalent impedance analyzer line parameter identification techniques have been described in [3,20]. The first is based on the modal decomposition of the MTL equations [9], and the second is based on their non-diagonalized form. This paper introduces an experimental protocol for impedance analyzer-based parameter identification using the same formulation as on [20], and for convenience, its measurement process is resumed here.

The cable parameters can be obtained from short-circuited and open- ended input impedance measurements. The input impedance matrix of a short-circuited (SC) and an open-ended (OC) line are the following [1,20]:

$$\mathbf{Z}^{\mathrm{SC}}(0) = \mathbf{Z}_c\left[\cosh(\ell\sqrt{\mathbf{YZ}})\right]^{-1}\sinh(\ell\sqrt{\mathbf{YZ}}) \tag{8}$$

$$\mathbf{Z}^{OC}(0) = \mathbf{Z}_c\left[\sinh(\ell\sqrt{\mathbf{YZ}})\right]^{-1}\cosh(\ell\sqrt{\mathbf{YZ}}) \tag{9}$$

From Eqs. (8) and (9), the characteristic impedance $\mathbf{Z_c}$ and propagation matrix $\sqrt{\mathbf{YZ}}$ can be obtained with:

$$\mathbf{Z}_c = \left\{\mathbf{Z}^{\mathrm{SC}}(0)\left[\mathbf{Z}^{OC}(0)\right]^{-1}\right\}^{-1/2}\mathbf{Z}^{\mathrm{SC}}(0) \tag{10}$$

$$[\cosh(\ell\sqrt{\mathbf{YZ}})]^{-1}\sinh(\ell\sqrt{\mathbf{YZ}}) = \mathbf{Z}_c^{-1}\mathbf{Z}^{\mathrm{SC}}(0) \tag{11}$$

Equation (11) was solved numerically to obtain $\sqrt{\mathbf{YZ}}$.

The input impedance matrices $\mathbf{Z}(0)$ can be obtained through measurements using an impedance analyzer. The diagonal elements of the matrix can be measured directly using the setup presented in Fig. 2, under the condition that

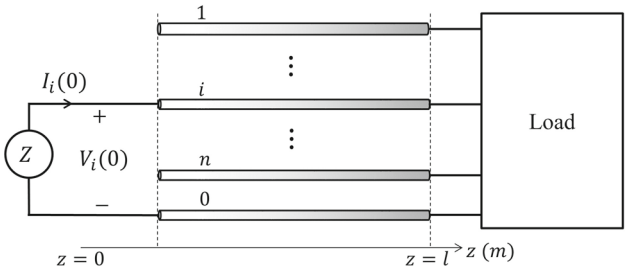

Fig. 2 Self-impedance measurement setup

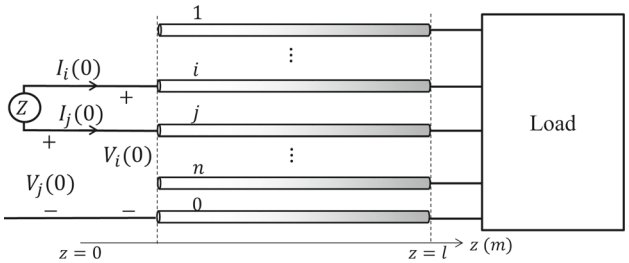

Fig. 3 Mutual-impedance measurement setup

all conductor currents are zero at $z = 0$ except on the conductors under test:

$$Z_{ii}(0) = \frac{V_i(0)}{I_i(0)} \tag{12}$$

The non-diagonal elements cannot be directly measured. However, they can be obtained from the measurement setup presented in Fig. 3 using (14) [20], where Z_{Mij} is the impedance measured between conductors i and j, when the current in the other conductors at $z = 0$ is null:

$$Z_{Mij}(0) = \frac{V_i(0) - V_j(0)}{I_i(0)} \tag{13}$$

$$Z_{ij}(0) = \frac{1}{2}(Z_{ii}(0) + Z_{jj}(0) - Z_{Mij}) \tag{14}$$

Once all possible combination of two distinct conductors has been measured, the input impedance matrix can be filled. In the general case, n self-impedance and $n(n-1)/2$ mutual-impedance measurements are required to complete it. If special conditions such as circular symmetry—case in which the elements of $\mathbf{Z}(0)$ repeat cyclic [24]—are verified, the number of measurements required can be reduced.

4 Measurement protocol

In this section, the protocol to guarantee the accuracy of the input impedance measurements of unshielded cables is described. The measurements with unshielded cables in the medium frequency band require special precautions that have

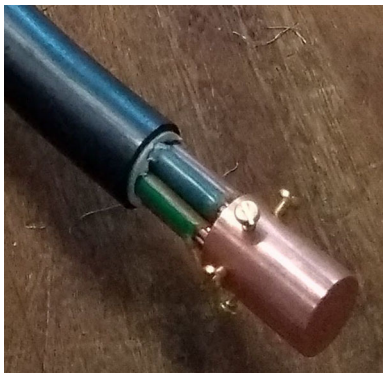

Fig. 4 Copper short-circuit terminal for 5 conductor cable

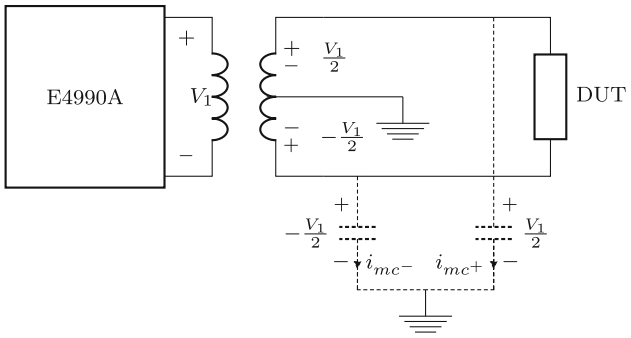

Fig. 5 Common-mode analysis of balun-isolated measurement

not yet been discussed in the literature. These precautions are detailed in the following subsection.

4.1 Parameter identification in the medium frequency band

In the medium frequency band, the resonance of a few meters long cable occurs. Indeed, the propagation velocity on power cables is usually $v = c/2$, where c is the speed of light. For example, the first resonance of an $\ell = 10$-m-long cable occurs around $f = v/4\ell = 3.75\,\text{MHz}$.

If resonance occurs on the sample cable in the frequency band of the identification measurements, the accuracy of the parameters around the resonance frequency is highly dependent on the quality of the short-circuit connection, and on whether it changes the equivalent length of the cable (in relation to the open circuit length). To minimize this problem, the short circuit must be carefully performed. The best practice would be to use massive connector made of conducting materials, such as the copper terminal in Fig. 4, to minimize impact of the short circuit on the equivalent cable length and guarantee that the connection has a near zero impedance.

The second problem impacts exclusively unshielded cables: An open-ended unshielded cable behaves as an antenna for frequencies higher than $f > v/4\ell$. Even if it could be considered a poor antenna, any electromagnetic waves propagating in the environment may be captured by the cable and induced an important error on the impedance measurements. Therefore, if the desired frequency band includes frequencies higher than $f > v/4\ell$, the measurements have to be taken inside a metallic cage that can provide a clean electromagnetic environment, e.g., Faraday cage, anechoic chamber, etc.

Moreover, if the measurements are taken inside a metallic cage, the sample cable must be placed away from the floor and walls. Indeed, if the cable is close to any metallic surface, Foucault currents will be produced, affecting the identification of the magnetic coupling between the conductors, and the stray capacitances between the conductors and the surface would be in parallel with the p.u.l. capacitances of the cable, compromising the accurate identification of the latter.

The last problem to be treated in this frequency band is the common mode, which generates stray currents that escape the measurement circuit. The common-mode currents increase with frequency, as they flow through stray capacitances between the cable and any conductive object nearby.

An efficient technique to mitigate the common-mode circulation is to balance the voltage on the input of the cable, using a balanced to unbalanced transformer, known as balun. The principle of this solution is represented in Fig. 5: The middle point of the secondary of the transformer is connected to the mass, which allows symmetric voltages on its output. The common-mode currents generated by balanced voltages have the same magnitude, and flow on opposite directions, thus canceling each other. The three-measurement impedance analyzer compensation (OPEN, SHORT and LOAD) has to be performed at the balun output.

To sum up, it is best to avoid the resonance phenomena on the sample cable during the impedance measurements by choosing a sample cable short enough. If reducing the sample cable length is not a viable option and resonance does occur in the identification measurements, these should be performed inside a metallic cage. Independent of the resonance, a balun should be used to balance the voltage on the cable input, the cable should be placed away from any metallic surface, and the short circuit should be performed with a massive conducting terminal. This protocol is a contribution to the current literature as the measurement problems specify to unshielded power cables, such as the radiation interference has not yet been discussed, and it resumes all precautions needed for an accurate impedance measurement in long cables.

4.2 Parameter identification in the low frequency band

In low frequencies, typically up to a few hundreds of kHz, resonance is not likely to occur in a few meters long cable,

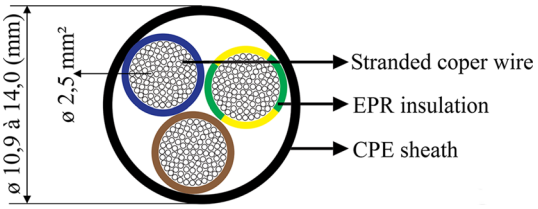

Fig. 6 Three-conductor cable cross section

Table 1 Sample cable length for each frequency band

	Sample length
DC—500 kHz	12 m
500 kHz–10 MHz	1 m

and the common-mode currents can be considered negligible. Indeed, the stray capacitances between the conductors and the surrounding environment (floor, walls, etc.) are of the order of 10 pF (cf. "Appendix"), and have an impedance of the order of tens of kΩ in this frequency band. Therefore, the balun is not necessary, and there is no need of a clean electromagnetic environment to perform the input impedance measurements.

In low frequency, the main source of inaccuracy is the fact that the input impedance of a short-circuited cable is very low, and the open-ended cable one is very high. The accuracy of the measurement with impedance analyzer is optimal only between 50 Ω and 10 kΩ [18]. For that reason, it is a good practice to use a cable as long as possible for the parameter identification in low frequency, so that the measured impedances are closer to this interval and thus more accurate.

In DC, the p.u.l. resistance and conductance should preferably be measured with an association of high-accuracy voltmeter and ammeter, favoring the connection that minimizes their insertion error.

4.3 Example of cable parameter identification

In this section, the parameter identification of a three-conductor unshielded cable, with conductors of section 2.5 mm^2, is described. The accuracy of the cable parameters will be validated experimentally in the frequency and time domains in Sects. 5 and 6.

The three-conductor cable cross section is represented in Fig. 6. For applications where cable are excited through silicon-based power converters, the rise and fall time of the excitation should be around hundreds of ns, which means it injects harmonics up to tens of MHz. This cable parameters are identified from DC up to 20 MHz. Two sample cable lengths were chosen, one for the low frequency band, and another for the high frequency band, as resumed in Table 1. Both samples were kept at least $1m$ away from any metallic surface during the impedance measurements. The high frequency sample is small enough to avoid radiation in this frequency band, and the metallic cage was not necessary.

The p.u.l. parameters of this cable are plotted in Fig. 7. In the figure, the black-dotted line indicates $f = 500$ kHz, the frequency at which the switch between the long sample cable and short sample cable is effectuated. The conductors are denominated 0, 1 and 2. A single number i in the subscript indicates a self-parameter of conductor i, and two numbers in the subscript ij indicated a coupling parameter between conductors i and j. The green-dotted lines show the parameters obtained from the 1-m sample cable identification for frequencies lower than 500 kHz: The error of this data tends to be bigger because they are taken at the limit of the balun frequency band. The purple-dotted line shows the parameters that are obtained with the 12-m-long cable for frequencies higher than 500 kHz: In this frequency band, the risk of errors due to common mode on the long cable input impedance measurement is higher.

The characteristic impedance matrix of the cable is represented in Fig. 8, where $\mathbf{Z_{c}}_{11}$ and $\mathbf{Z_{c}}_{22}$ are the diagonal elements of the matrix, and $\mathbf{Z_{c}}_{12}$ and $\mathbf{Z_{c}}_{21}$ are the non-diagonal elements.

The p.u.l. capacitance in a transmission line is usually considered constant in the literature, but in this cable, it presents a small decrease with frequency (Fig. 7d). This behavior is due to a slight frequency dependence of the dielectric constant of the EPR insulation of the cable, as formerly evidenced in [12]. In any case, to ensure that this variation is due to the insulation dielectric behavior and not to a measurement error, the p.u.l. capacitance between two conductors was measured using the spectrometer Novocontrol "Alpha-A High Performance Frequency Analyzer," and the results are plotted in Fig. 9. The spectrometer confirmed that the p.u.l. capacitance in this cable decreases with frequency.

Discontinuities are visible in the p.u.l. parameters at 500 kHz. They are due to the change in the sample cable, and in Sect. 6, it will be shown that accurate results can be obtained from these parameters despite these discontinuities. The p.u.l. resistance presents the strongest variation. It depends strongly on the real part of the input impedance of the short-circuited cable. The discontinuity on the resistance is more important because the short-circuited 12-m-long sample cable impedance is highly inductive at 500 kHz, what reduces the accuracy of the measurement of its real part. Indeed, if the imaginary part of the measured impedance is considerably higher than the real part, the intrinsic error of the measured phase impacts strongly the accuracy of the real part.

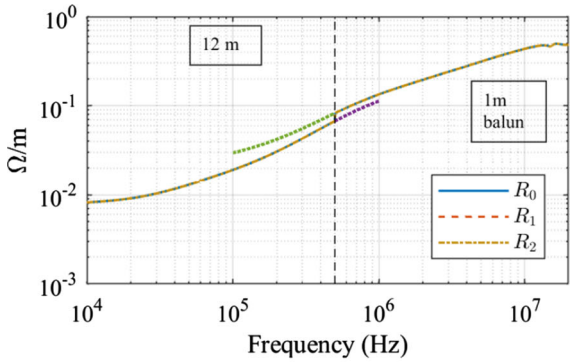

(a) p.u.l. resistance

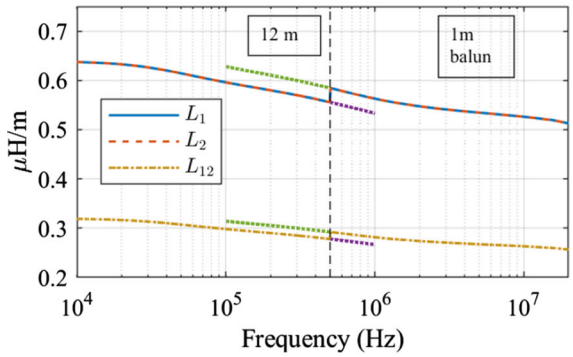

(b) p.u.l. inductance

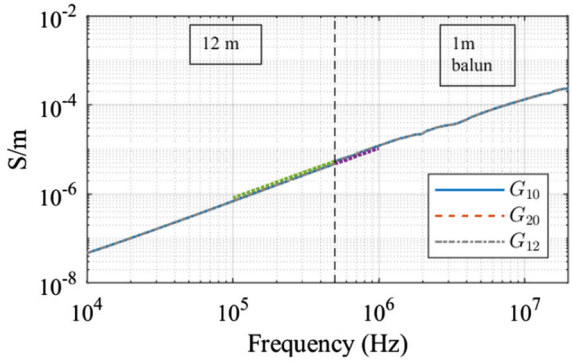

(c) p.u.l. conductance

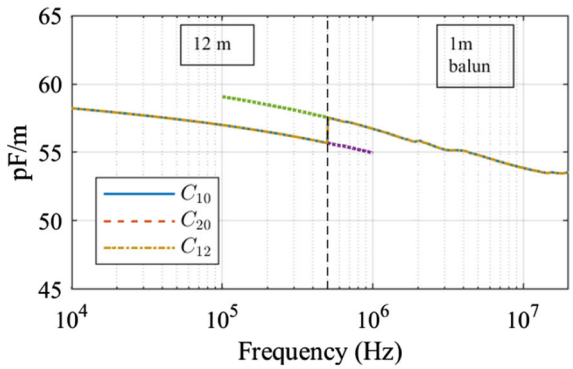

(d) p.u.l. capacitance

Fig. 7 Three-conductor cable p.u.l. parameters dotted green line: extension of the 1-m-long sample cable parameters under 500 kHz and dotted purple line: extension of the 12 m over 500 kHz (colour figure online)

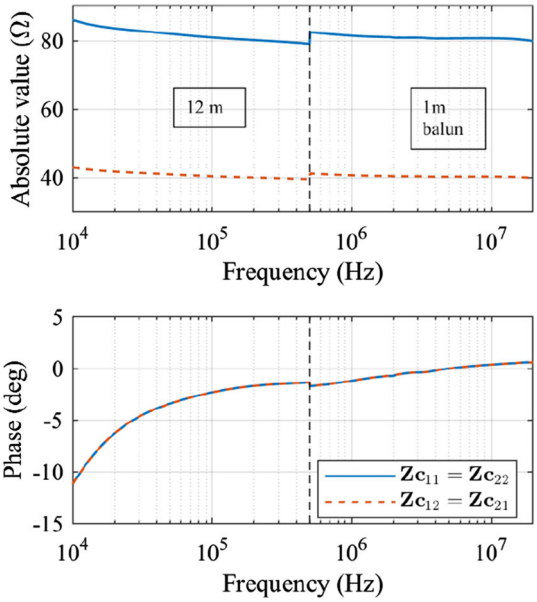

Fig. 8 Characteristic impedance

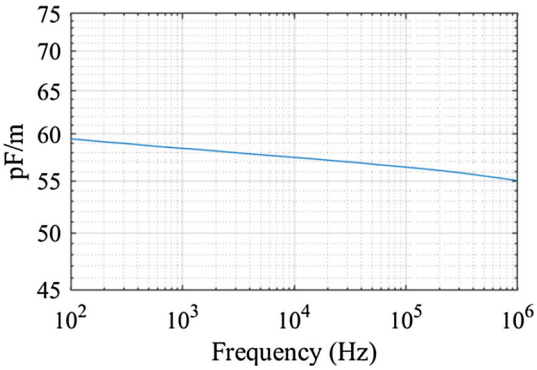

Fig. 9 p.u.l. capacitance measured with impedance spectrometer

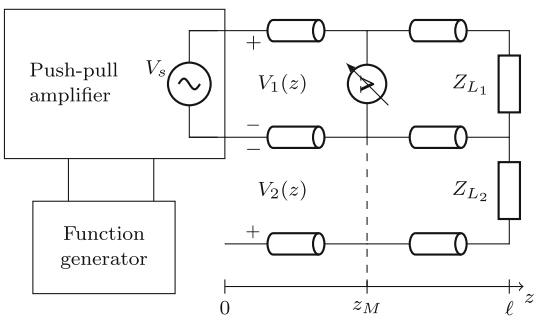

Fig. 10 Schematic of the frequency-domain validation experiment, $\ell = 12$ m

5 Frequency-domain validation

This section presents a frequency-domain validation experiment to determine the accuracy of the identified parameters. The schematic of the experiment is presented in Fig. 10. It consists of the injection of a sinusoidal voltage signal on the

input of a 12-m-long cable and the measurement of the voltage V_1 at position $z = z_M$. The experiment is performed between 1 and 10 MHz, where the first resonances of the 12-m-long cable take place. The theoretical determination of the frequency at which the resonance takes place is very sensitive to the accuracy of the cable parameters p.u.l. inductance and capacitance. Also, the determination of the amplification of the voltage at the resonance frequencies is highly dependent on accuracy of the loss-related parameters, p.u.l. resistance and conductance. Therefore, any possible inaccuracy present in cable parameters in Fig. 7 would be the most visible in the prediction of the voltage amplified by resonance, at the resonance frequencies of the cable.

The theoretical estimation of the voltage along the cable was done with the simulator described in Sect. 2, using the cable parameters plotted in Fig. 7.

To maximize the resonance-due voltage amplification, the experiment was designed with maximum reflection coefficients at the cable terminals. At $z = 0$, a push–pull amplifier with a closed-loop output was used to emulate a voltage source with near zero output impedance. At $z = \ell$, the loads are either short circuits or open ends. The experiment was performed for two load configurations:

- Configuration 1: open/short combination, $Z_{L_1} - > \infty$ and $Z_{L_2} = 0\ \Omega$;
- Configuration 2: complete short circuit, $Z_{L_1} = 0\ \Omega$ and $Z_{L_2} = 0\ \Omega$.

The position z_M at which the maximal voltage amplification occurs was predicted numerically. In configuration 1, the maximal voltage occurs at $z_M = \ell$, and in configuration 2, at $z_M = \ell/2$.

The scope used for the voltage measurements was fed through a battery, to avoid the possible common-mode path through the scope electrical plug. The cable and the scope were suspended with insulating supports to minimize common-mode currents during the experiment, which is shown in Fig. 14.

The experimental data, along with its accuracy interval, are plotted over the theoretical prediction of the voltage in Fig. 11. The results are plotted in terms of relative voltage amplification $V_1(z)/V_1(0)$.

The theoretical model presents a good agreement with the experimental data. It can be concluded that the parameter identification detailed in Sect. 4.3 has a good accuracy.

The frequency-domain simulation allows a numerical analysis of the impact of the accuracy of the loss-related parameters when the resonance behavior of a MTL is to be theoretically predicted. In Fig. 12, the theoretical voltage amplification in configuration 1 (open/short) has been plotted using three different set of parameters. The first set is the frequency-dependent parameters in Fig. 7. The other

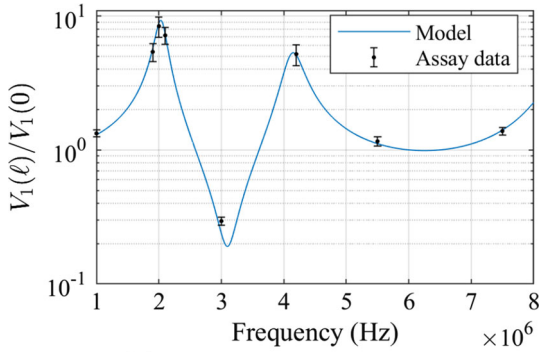

(a) Configuration 1: Open/Short

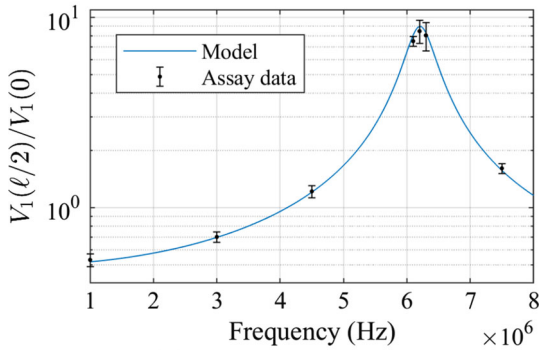

(b) Configuration 2: Short

Fig. 11 Experimental validation on frequency domain: resonance-due voltage amplification

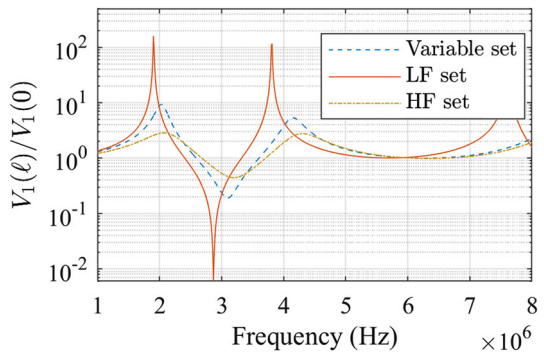

Fig. 12 Effect of the loss-related parameters on the voltage amplification

two sets have parameters constant with frequency, and they are denominated "LF" (low frequency) and "HF" (high frequency) and are detailed in Table 2. The "LF" has the DC values of the loss-related parameters R_i and G_{ii}, and the reactive parameters L_{ii} and C_{ii} are evaluated at 50 kHz, while the "HF" set has all the parameters evaluated at 10 MHz.

The results in Fig. 12 show the importance of taking the frequency dependence of the parameters into account. The resonance-due voltage amplification and the resonance frequency can be correctly calculated exclusively with frequency-dependent parameters. Indeed, the resonance frequency is sensitive to the variation in the p.u.l. inductance

Table 2 Fixed cable parameters for resonance analysis

	R_i	L_{ii}	G_{ii}	C_{ii}
LF (DC, 50 kHz)	$13.4\frac{\text{m}\Omega}{\text{m}}$	$547\frac{\text{nH}}{\text{m}}$	$1\frac{\text{nS}}{\text{m}}$	$58\frac{\text{pF}}{\text{m}}$
HF (10 MHz)	$435\frac{\text{m}\Omega}{\text{m}}$	$526\frac{\text{nH}}{\text{m}}$	$133\frac{\mu\text{S}}{\text{m}}$	$54\frac{\text{pF}}{\text{m}}$

with frequency and variation due to proximity and skin effects.

6 Time-domain analysis

6.1 Frequency-domain simulation results converted to time domain

To avoid the need to represent the frequency dependence of the cable parameters in Fig. 7 on time domain, the proposed model consists in simulating a system in the frequency domain and converts the simulation results back to time domain. By avoiding equivalent circuits or other to represent the frequency dependence of the parameters, the accuracy of the exact solution of the telegrapher equations (cf. Sect. 2) is preserved.

The case of systems with periodic excitation, such as power converters, is analyzed. The conversion to frequency domain is done via a Fourier series decomposition followed by the phasor transform. The power converters can be represented by piece-wise linear periodic sources, as demonstrated in [10,26,27]. Once the frequency simulation is complete, the results can be easily transformed back to time domain.

This is the simplest model able to take into account the frequency dependence of the cable parameters. Its main advantages are that it is numerically efficient, its computing time does not depend on the cable length, no approximations are needed to represent the cable parameter frequency dependence, and effects such as the propagation delay are correctly represented. The methodology proposed here can be applicable to any system with periodic excitation and can be extended to the general case via the Fourier transform.

6.2 Time-domain validation

A time-domain validation experiment was designed to validate the modeling technique presented in Sect. 6.1, as well as the accuracy of the cable parameters in whole frequency band, from DC up to 10 MHz. The experimental setup is described in Fig. 13. It consists in a 12-m-long cable excited by an inverter leg. The cable terminal is a passive load, inductive in differential mode and capacitive in common mode. This system is similar to a motor connected to its drive

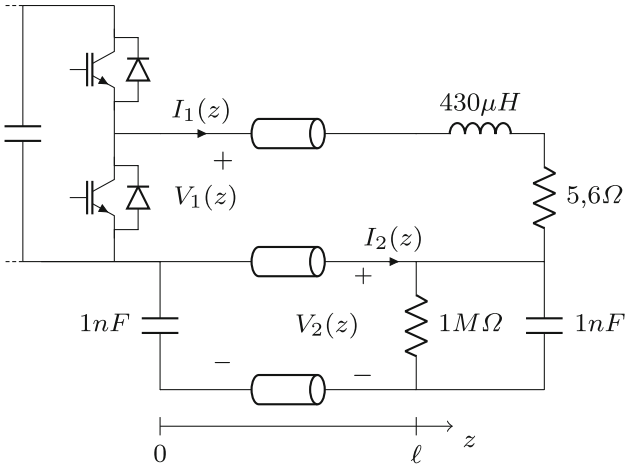

Fig. 13 Schematic for the three-conductor cable time-domain validation experiment, $\ell = 12\,\text{m}$

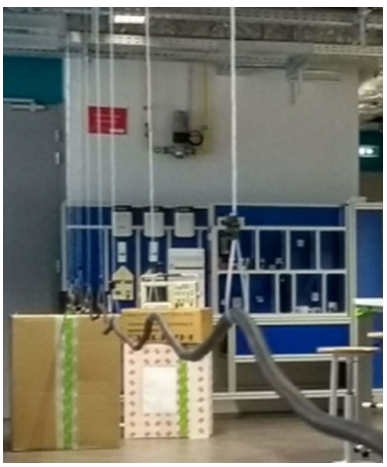

Fig. 14 Experimental setup

through a long cable, and dangerous resonance-due overvoltages and overcurrents can occur at the cable extremities.

In this experiment, two variables were measured: the voltage at $z = \ell$ and the current at $z = 0$, each in the position of their maximal amplification due to resonance. The DC components of these variables were measured with DC voltmeter and ammeter, to increase their accuracy. The measurements were taken independently, with only one probe connected at a time.

Precautions were taken to mitigate common-mode circulation on the experimental setup, such as suspending the cable with insulating supports, as shown in Fig. 14. Indeed, the authors assessed that the common mode affects slightly the resonance frequency of the cable, because it behaves as a fourth conductor in the MTL. The load connected at $z = \ell$ is shown in Fig. 15.

This system was simulated on frequency domain, and its results are converted to time domain as described in Sect. 6.1. The time-domain voltages at $z = \ell$ and currents at $z = 0$ are

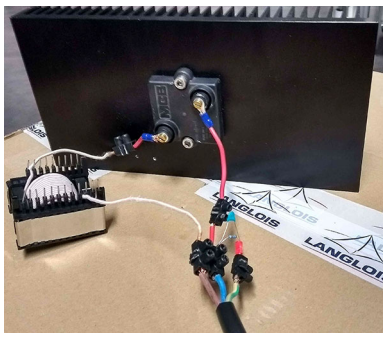

Fig. 15 Load used in the three-conductor cable time-domain validation experiment

plotted over the experimental data in Fig. 16. The absolute error between the theoretical and experimental results is plotted in Fig. 17.

The theoretical results present a good agreement with the experimental data, the only discrepancy being a slight difference on the frequency of the oscillations, which causes a few points in Fig. 17 to be out of the scope accuracy limit. As aforementioned, common-mode currents are the cause of this difference, and the precautions taken to mitigate it (cf. Fig. 14) significantly reduced the oscillation frequency discrepancy but were not sufficient to completely cancel the common mode in the experimental setup.

In this study case, it is also possible to analyze the impact of constant cable parameters in the result accuracy. In Fig. 18, the time-domain results obtained from three different sets of parameters are plotted. The sets are the same from the analysis performed in the previous section: The first has the variable parameters in Fig. 7, and the other two the fixed parameters in Table 2.

The results obtained from the low frequency parameters have an attenuation much inferior to the complete model, whereas those from high frequency parameters have an attenuation considerably higher, and a voltage drop in the first phase of the switching period much higher than expected. This voltage drop is present because the 20 MHz losses are (considerably) greater than the DC losses.

The results in Fig. 18 show clearly the importance of an accurate modeling of the cable losses when resonance phenomenon takes place in a cable. It is the fact that R and G are variables with the frequency that guarantees the adequate end value of the voltage in each phase of the switching period, and at the same time a realistic attenuation of the resonance-due oscillations.

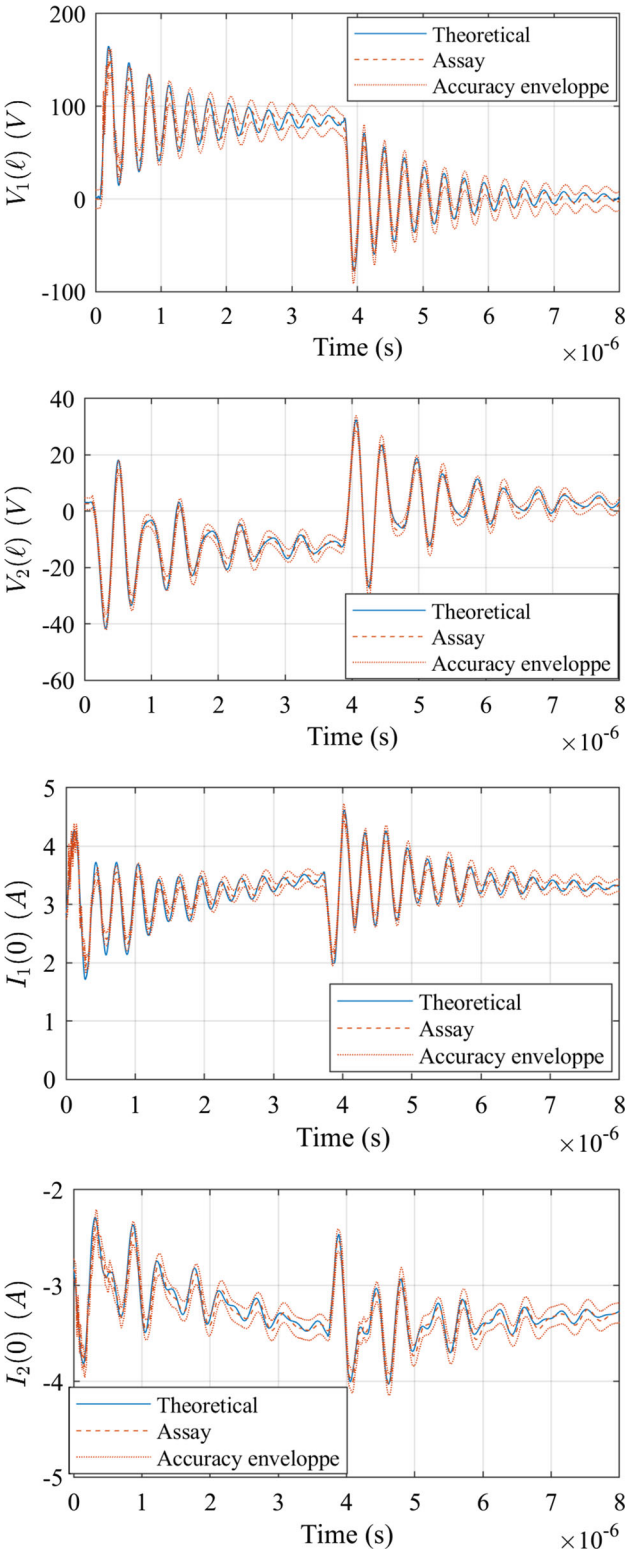

Fig. 16 Time-domain validation results

7 Conclusion

The simulation on frequency domain followed by the conversion to time domain, as proposed in this paper, is a

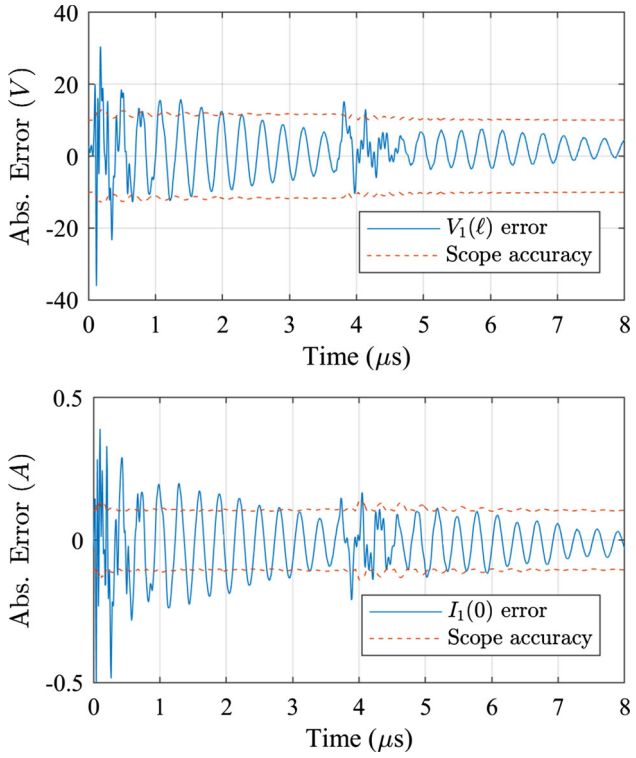

Fig. 17 Absolute error on time-domain validation, between theoretical and experimental results

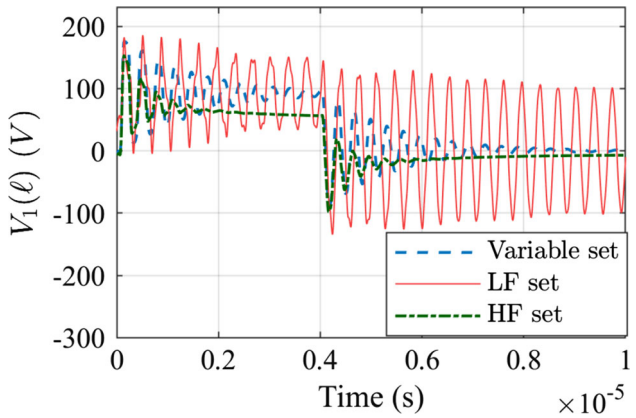

Fig. 18 Comparison between different loss modeling

straightforward method to model long cables in which resonance takes place. Its main advantages are: its efficiency and accuracy, the later depending only on the accuracy of the cable parameters; the fact that the simulation time does not depend on the cable length; and the accurate representation of phenomena such as the wave travel delay. The parameter identification protocol described in this paper allows the accurate determination of unshielded cable parameters in a large frequency band. This paper presents a complete modeling technique for unshielded cables well suited for applications where long cables are excited by power converters, having a light numerical cost and modeling accurately the cable resonance behavior.

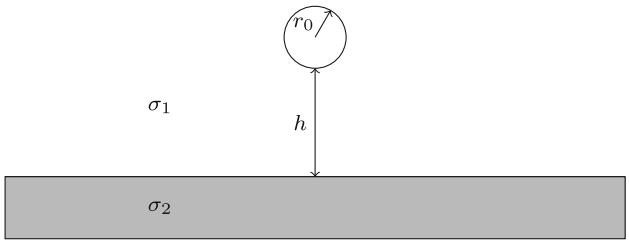

Fig. 19 Schematic for the capacitance calculation

Acknowledgements The authors would like to thank Dr. Mario Leite from IPT (Institute of Technological Research, São Paulo, Brazil) for his help on measurements that contributed to this paper.

Appendix

The estimation of the stray capacitance between the cable conductors and a concrete plane (floor, walls) can be done using the PEEC technique described in [5,6]. This method was applied to calculate the capacitance of a wire of radius r_0 and length ℓ parallel to a concrete ground, placed at a distance h above the ground, as shown in Fig. 19. In the figure, σ_1 is the complex conductivity of the air and σ_2 is the complex conductivity of the concrete. The capacitance between the wire and the concrete surface can be calculated with Eqs. (15) to (18).

$$C_{\mathrm{CM}} = -\frac{1}{\mathbf{Im}(Z_{\mathrm{CM}})\omega} \tag{15}$$

$$Z_{\mathrm{CM}} = Z_1 + Z_2 \tag{16}$$

$$Z_1 = \frac{1}{2\pi\ell\sigma_1}\left[\ln\left(\frac{\ell+\sqrt{\ell^2+r_0^2}}{r_0}\right) + -\sqrt{1+\left(\frac{r_0}{\ell}\right)^2}+\frac{r_0}{\ell}\right] \tag{17}$$

$$Z_2 = \frac{1}{2\pi\ell\sigma_1}\frac{\sigma_1-\sigma_2}{\sigma_1+\sigma_2}\left[\ln\left(\frac{\ell+\sqrt{\ell^2+r_0^2}}{r_0+2h}\right) + -\sqrt{1+\left(\frac{r_0+2h}{\ell}\right)^2}+\frac{r_0+2h}{\ell}\right] \tag{18}$$

As an example, suppose the section of the wire is 2.5 mm^2, its length $\ell = 1$ m, and it is placed at $h = 1$ m. In this case, the stray capacitance between the wire and the concrete floor ($\sigma_2 = 2.5$ mS/m) would be:

$$C_{CM} = 8.6\,pF$$

Based on this example, the stray capacitances in the impedance measurement set were estimated to be of the order of 10 pF along the document.

References

1. Agrawal AK, Lee K, Scott LD et al (1979) Experimental characterization of multiconductor transmission lines in the frequency domain. IEEE Trans EMC 21:28–32
2. Batura R, Opydo W (2005) Overvoltages caused by switching unloaded cable lines by a vacuum switch. Electr Eng 87(4):181–189. https://doi.org/10.1007/s00202-004-0238-2
3. Brandão JA, das Neves MG (2011) Basic principles concerning the experimental evaluation of the frequency-dependent parameters of shielded and unshielded three-phase symmetric cables. IEEE Trans Power Deliv 26:556–564
4. Chu X, Lin F, Yang Z (2014) The analysis of time-varying resonances in the power supply line of high speed trains. In: International power electronics conference
5. Clavel E, Roudet J, Guichon J et al (2018) A nonmeshing approach for modeling grounding. IEEE Trans EMC 60(3):795–802. https://doi.org/10.1109/TEMC.2017.2743227
6. Clavel E, Roudet J, Hayashi Feuerharmel A, et al (2019) Benefits of the ground peec modeling approach—example of a residential building struck by lightning. IEEE Trans EMC. pp 1–9. https://doi.org/10.1109/TEMC.2019.2898234
7. Cristina S, Feliziani M (1989) A finite element technique for multiconductor cable parameters calculation. IEEE Trans Magn 25:2986–2988
8. Gao Z, Ji R, Zhang X, et al (2016) Finite-element modeling and impedance characteristics analysis of two parallel cables in aircraft power system. In: 2016 IEEE/CSAA international conference on aircraft utility systems (AUS), Beijing
9. Gentili GG, Salazar-Palma M (1995) The definition and computation of modal characteristic impedance in quasi-TEM coupled transmission lines. IEEE Trans Microw Theory Tech, pp 338–343
10. Gómez P, Uribe FA (2009) The numerical Laplace transform: an accurate technique for analyzing electromagnetic transients on power system devices. Int J Electr Power Energy Syst 31(2):116–123. https://doi.org/10.1016/j.ijepes.2008.10.006
11. Gong X, Ferreira JA (2014) Comparison and Reduction of conducted EMI in SiC JFET and Si IGBT-based motor drives. IEEE Trans Power Electron 29(4):1757–1767. https://doi.org/10.1109/TPEL.2013.2271301
12. Guo JJ, Boggs SA (2011) High frequency signal propagation in solid dielectric tape shielded power cables. IEEE Trans Power Deliv 26(3):1793–1802. https://doi.org/10.1109/TPWRD.2010.2099134
13. Habib S, Kordi B (2013) Calculation of multiconductor underground cables high-frequency per-unit-length parameters using electromagnetic modal analysis. IEEE Trans Power Deliv 28:276–284
14. Honarbakhsh B, Asadi S (2017) Analysis of multiconductor transmission lines using the CN-FDTD method. IEEE Trans EMC 59:184–192
15. Hosoya M (2000) The simplest equivalent circuit of a multiterminal network. Bull Fac Sci Univ Ryukyus 70:1–10
16. Idir N, Weens Y, Franchaud JJ (2009) Skin effect and dielectric loss models of power cables. IEEE Trans Dielectr Electr Insul 16(1):147–154. https://doi.org/10.1109/TDEI.2009.4784562
17. Kerkman RJ, Skibinski DLGL (1997) Interaction of drive modulation and cable parameters on AC motor transients. IEEE Trans Ind Appl 33(3):722–731. https://doi.org/10.1109/28.585863
18. Keysight Technologies: E4990A Impedance Analyzer—Data Sheet (2018). https://literature.cdn.keysight.com/litweb/pdf/5991-3890EN.pdf?id=2459964. Accessed 11 Jan 2019
19. Kim JH, Oh D, Kim W (2010) Accurate characterization of broadband multiconductor transmission lines for high-speed digital systems. IEEE Trans Adv Packag 33:857–867
20. Knockaert J, Peuteman J, Catrysse J et al (2010) A vector impedance meter method to characterize multiconductor transmission-line parameters. IEEE Trans EMC 52:1019–1025
21. Kruizinga B, Wouters PAAF, Steennis EF (2015) High frequency modeling of a shielded four-core low voltage underground power cable. IEEE Trans Dielectr Electr Insul 22:649–656
22. Marlier C, Videt A, Idir N (2015) NIF-based frequency-domain modeling method of three-wire shielded energy cables for EMC simulation. IEEE Trans EMC 57(1):145–155. https://doi.org/10.1109/TEMC.2014.2359514
23. Moreira AF, Lipo TH, Venkataramanan G et al (2002) High-frequency modeling for cable and induction motor overvoltage studies in long cable drivers. IEEE Trans Power Electron 25:1297–1306
24. Paul C (2008) Analysis of multiconductor transmission lines. IEEE Press, New Jersey
25. de Paula H, de Andrade DA, Chaves MLR et al (2008) Methodology for cable modeling and simulation for high-frequency phenomena studies in pwm motor drives. IEEE Trans Power Electron 23:744–752
26. Revol B, Roudet J, Schanen J et al (2011) Emi study of three-phase inverter-fed motor drives. IEEE Trans Ind Appl 47(1):223–231
27. Scheich R, Roudet J, Bigot S et al (1993) Common mode RFI of a HF power converter: phenomena, its modelling and its measurement. In: EPE'93
28. Sousounis MC, Shek JKH, Mueller MA (2016) Filter design for cable overvoltage and power loss minimization in a tidal energy system with onshore converters. IEEE Trans Sustain Energy 7:400–408
29. Stevanović I, Wunsch B, Madonna GL et al (2014) High-frequency behavioral multiconductor cable modeling for emi simulations in power electronics. IEEE Trans Ind Inf 10:1392–1400
30. Uribe FA, Flores J (2018) Parameter estimation of arbitrary-shape electrical cables through an image processing technique. Electr Eng 100(3):1749–1759. https://doi.org/10.1007/s00202-017-0651-y
31. Wang L, Avolio G, Deconinck G et al (2014) Estimation of multiconductor powerline cable parameters for the modelling of transfer characteristics. IET Sci Meas Technol 8:39–45. https://doi.org/10.1049/iet-smt.2012.0123
32. Wang L, Ho CN, Canales F et al (2010) High-frequency modeling of the long-cable-fed induction motor drive system using TLM approach for predicting overvoltage transients. IEEE Trans Power Electron 25(10):2653–2664. https://doi.org/10.1109/TPEL.2010.2047027
33. Weens Y, Idir N, Bausière R et al (2006) Modeling and simulation of unshielded and shielded energy cables in frequency and time domains. IEEE Trans Magn 44:1876–1882
34. Williams DF (1997) Multiconductor transmission line characterization. IEEE Trans Compon Packag Manuf Technol 20:129–132
35. Wunsch B, Stevanović I (2017) Length-scalable multi-conductor cable modeling for EMI simulations in power electronics. IEEE Trans Power Electron 32:1908–1916
36. Zhang S, Jiang S, Lu X et al (2014) Resonance issues and damping techniques for grid-connected inverters with long transmission cable. IEEE Trans EMC 29:110–120